Microsc. Microanal. 18, 1–7, 2012
doi:10.1017/S1431927612001262

Microscopy AND Microanalysis

Shedding New Light on Cathodoluminescence—A Low Voltage Perspective

Natasha Erdman,* Charles Nielsen, and Vernon E. Robertson

JEOL USA Inc., 11 Dearborn Rd., Peabody, MA 01960, USA

Abstract: Previously, imaging and analysis with cathodoluminescence (CL) detectors required using high accelerating voltages. Utilization of lower accelerating voltage for microanalysis has the advantages of reduced beam-specimen interaction volume, and thus better spatial resolution, as well as reduction in electron beam induced damage. This article will highlight recent developments in field emission gun–scanning electron microscope technology that have allowed acquisition of high spatial resolution CL images at very low accelerating voltages. The advantages of low kV CL imaging will be shown using examples of a geological specimen (shale) and a specimen of an industrial grade diamond.

Key words: cathodoluminescence, low voltage, FEG-SEM, panchromatic

Introduction

Scanning electron microscopes have historically been operated at relatively high voltages, between 15–40 kV; however, recent instrumental developments provide ultralow voltage imaging on the order of tens of volts of accelerating voltage. The two most obvious advantages of low voltage imaging and analysis are:

1. The ability to reduce electron beam-specimen interaction volume from several microns to a few 10s or 100s of nm, thus providing substantially more surface-specific information for both secondary and backscatter imaging. At higher voltages, it may be difficult to discern which features are located subsurface, whereas using a lower voltage will eliminate such ambiguity. Lower accelerating voltage also improves the lateral spatial resolution in terms of where the signal comes from.
2. Substantial reduction in specimen damage as a result of the electron beam interaction. This is a particularly important point while conducting microanalyses because large probe currents are typically employed for prolonged periods of time, and care should be taken not to expose specimens to excessive beam current or accelerating voltage.

The key aspect of high spatial resolution microanalysis is the ability to deliver high probe current in a very small probe with the correct shape while operating at low voltage to reduce beam/specimen interaction volume. Therefore, recent microscope developments have been focused on both improving electron source design to deliver the highest available current at a given accelerating voltage as well as improvement of lens design to maintain the smallest probe diameter. One of the approaches employed in the JEOL field emission gun–scanning electron microscopes (FEG-SEMs) to increase the amount of probe current delivered to the specimen at any given kV is to use an "in-lens" electron gun. In this design the electron source is placed inside the magnetic field of a low aberration condenser lens, which is integrated with the anodes of the FEG. The high brightness electron beam is confined into a narrow angle and passes through the anode aperture, and then is converged into a small spot by the subsequent objective, thus creating a system capable of delivering ten times higher current (200–400 nA) than the conventional FEG systems. The aperture angle control lens (ACL) that is incorporated in the column just above the objective lens ensures that not only can such a gun deliver a high probe current, but it also maintains a small probe size of the correct shape at the same time (Fig. 1). This lens design improvement translates into the ability to perform microanalysis at lower kVs without sacrificing probe size or probe current (for example, it is possible to obtain a 5 nm spot in 5 nA beam at 3 kV) and hence is particularly useful for cathodoluminescence (CL), energy dispersive spectrometer (EDS), and wavelength dispersive spectrometer (WDS) analysis at low voltages.

The ACL works by taking into account effects of all aberrations and diffraction on spot size and by optimizing the convergence angle accordingly in an automatic fashion. When the SEM is optimized for the smallest probe size (largest conversion angle), some beam scatter (and X-ray generation) away from the immediate probe is possible due to the large Cs value; this is insignificant for low beam current applications (such as basic high-resolution imaging). When the ACL is optimized for analytical work (smallest convergence angle), the ultimate probe size is slightly increased (but still well below the analytical generation volume); the analytical signal is no longer affected by the beam tailing, resulting in a smaller amount of signal delocalization. As an example, the probe resolution at 5 kV at analytical SEM working distance is 2.4 nm at 50 pA, 4.5 nm at 5 nA, and 12 nm at 100 nA. The key parameter for high spatial resolution microanalysis is not only probe size but probe shape as well.

Received February 29, 2012; accepted April 26, 2012
**Corresponding author*. E-mail: erdman@jeol.com

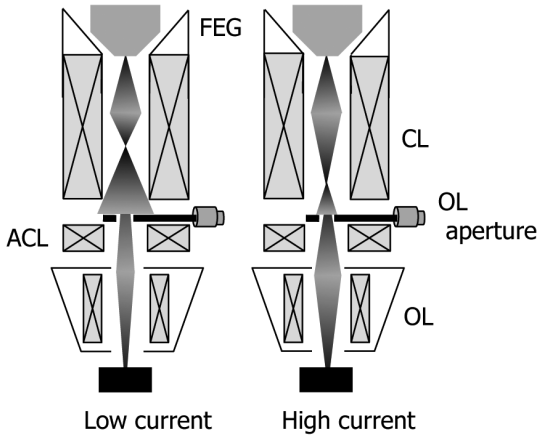

Figure 1. Principle of ACL operation. The ACL works by optimizing the convergence angle (α) over a range of accelerating voltages and probe currents to produce both the best imaging and analytical instrument performance.

In the past, imaging and analysis with CL detectors required using high accelerating voltages. The volume from which CL is generated can be minimized by reducing the accelerating voltage, hence improving the image resolution. It is well known that CL is produced by transitions between the conduction and valence bands and levels lying in the band gap. These transitions are often triggered by defects such as dopants (color centers on the ppb level) and material stress and strain. As such, CL images and spectra can reveal useful information about the material chemistry or growth history (Yacobi & Holt, 1990). CL intensity and spectrum sharpness can be enhanced at lower temperatures, but most studies now are performed at ambient temperatures due to the added cost and complexity of cryo-stages. There are currently several types of CL detection systems commercially available, and they consist of three basic components: the collection system, the sensor, and the spectrum analyzer. Each of these components is designed to satisfy a particular application.

The intensity of the CL emission will determine the type of collection system. For example, weak emissions from GaAs wafers require elaborate parabolic or ellipsoidal mirrors to collect as large of a solid angle as possible. They have a single opening for the electron beam and focus the CL to a fiber bundle or directly on to the sensor. These collection systems are often retractable as they may interfere with other SEM detectors such as backscattered electron (BSE) and EDS. Strong emitting materials such as zircons do not require special collectors, and the CL can often be detected directly by the sensor. The choice of sensor depends largely on the wavelength range of interest. The visible range is easily detected by photomultiplier tubes (PMTs) and silicon photodiodes. The near infrared band (0.74 to 1.4 μm) can be detected on special PMTs with cooled quartz windows, whereas longer wavelengths require solid state sensors such as PbS, Ge, InAs, and InSb.

CL detection systems are often divided into two classes: dispersive and nondispersive. Dispersive systems include spectrum analyzers that provide spectral information, whereas nondispersive systems output a signal proportional to the intensity and/or color of the entire range of emissions. Dispersive systems typically use a monochromator grating to scan through a range of wavelengths into a sensor to create a spectrum. The spectrum can be created either by mechanically tilting the grating with the diffracted light sensed by a PMT or solid state detector (serial collection) or by fixing the grating and collecting the light on a linear array of photodiodes (parallel collection). Both systems can produce CL maps or images as well as high-resolution spectra. The dispersive units can map the emission areas for a specific wavelength (monochromatic), whereas the nondispersive images show the emission areas from the entire range of wavelengths (panchromatic). Nondispersive systems may include a band-pass filter placed in front of the sensor that acts as a basic spectrum analyzer in that the output is now from a narrow band of wavelengths.

Adequate specimen preparation is an important aspect of successful and meaningful CL analysis, particularly at low voltages. In recent years significant advances in ion beam based preparation techniques have allowed preparation of complex geological materials (such as sedimentary rocks and shale) with minimal sample alteration or deformation, unlike previously utilized abrasive mechanical methods (Erdman et al., 2006). Defocused Ar ion cross-section polishing is an indispensable advancement for fine-scale SEM investigations of organic matter, mineral and pore distributions, and associations in highly consolidated geologic samples (Milner et al., 2010). Since major shale constituents such as organic material (OM), clay, quartz, carbonate, and pyrite exhibit various degrees of hardness, standard mechanical preparation (saw cutting, grinding, abrasive polishing, microtome cutting, etc.) tends to result in uneven surfaces due to abrasive smearing and/or pitting. This technique is also useful for preparation of materials that exhibit high level of strain and crystal defects, such as certain carbides and diamond grains; the crystallographic defects preserved during broad ion beam preparation can then further be analyzed using FEG-SEM and CL.

In this article we will present results of CL imaging using a panchromatic detector using an FEG-SEM on a variety of specimens, while emphasizing advantages of low voltage imaging and analysis. Some of the specimens we will discuss are both beam sensitive and have surface specific features (for example, shale), while other specimens are nonconductive (diamond); these considerations ultimately drive the imaging and the analysis into the low voltage regime.

Materials and Methods

Shale and polycrystalline diamond (PDC) samples were prepared using JEOL IB-09010 (JEOL USA, Inc., Peabody, MA, USA) broad argon ion beam cross polisher (Erdman et al., 2006). Several milligrams of pulverized material from the Woodford formation shale specimens were embedded

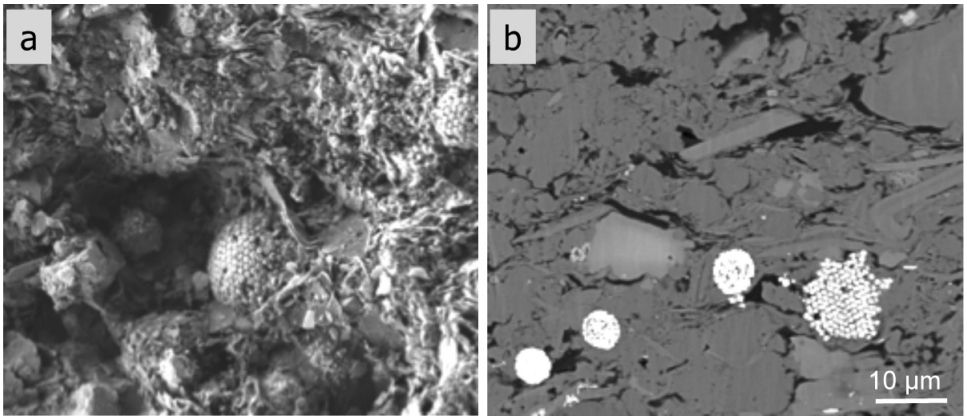

Figure 2. FE-SEM images of the Marcellus Shale specimen (**a**) before and (**b**) after ion beam polishing. The image on the left is taken with an E-T SE detector and shows a substantial amount of relief associated with mechanical abrasion. The image on the right (BSE) shows a smooth flat surface following ion milling.

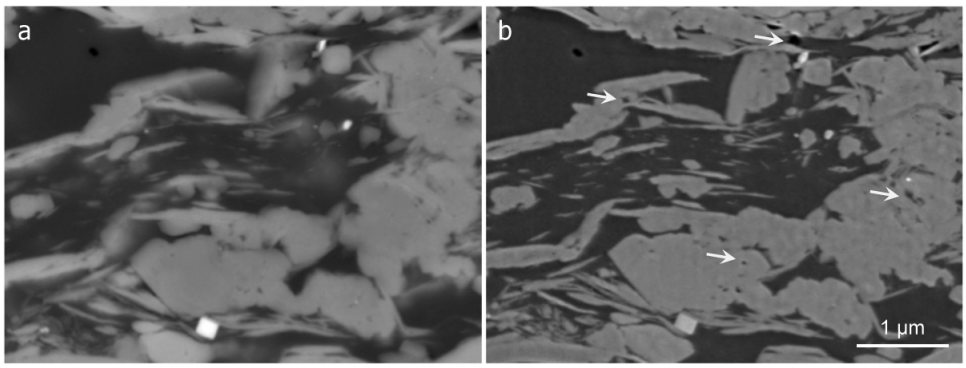

Figure 3. Comparison between (**a**) 8 kV and (**b**) 2 kV BSE observations of the Woodford Shale specimen. Arrows in image **b** highlight pores that were previously obscured by a large sampling volume at 8 kV.

in Epotek 353 ND epoxy resin (Epoxy Technology, Inc., Billerica, MA, USA) to mechanically stabilize them and polished using the CP at 5 kV for 4 h to produce a typical cross-sectioned area of 1.5 × 0.5 mm with minimal smearing or deformation. The shale samples were lightly carbon coated (less than 100 Å) using a JEOL JEE-420 evaporator prior to imaging and microanalysis to prevent specimen charging. The PDC specimen was ion polished using a rotation holder accessory at 8 kV for 3 h.

The JEOL JSM-7600F Schottky field emission SEM was used for imaging and microanalysis. The SEM is a semi-in-lens system, equipped with a low angle backscatter (LABe) detector. The panchromatic Centaurus CL detector (KE Developments, UK) containing a Hamamatsu PMT (Hamamatsu, Hamamatsu City, Japan) set to detect photons in the 185–850 nm range was utilized for CL imaging.

Results and Discussion

Shale

Figure 2 shows an example of a shale specimen polished with silicon carbide 1200 grit paper versus the same sample after ion beam polishing preparation. The comparison clearly demonstrates that inappropriate sample preparation will compromise attempts to image the exact locations of organic material (kerogen) and mineral grains along with both their internal and interfacial pore networks. Moreover, any CL signal will be difficult to interpret based on the highly uneven morphology of the mechanically polished specimen.

Figure 3 shows a comparison of BSE images taken at 8 kV and 2 kV for the same Woodford shale specimen. The arrows point to features observed at 8 kV that completely disappear at 2 kV following reduction in the beam-specimen interaction volume. This behavior can also be confirmed by utilizing the Monte Carlo simulations (Hovington et al., 1997) of beam interaction with C (kerogen), Si (quartz or clay), and Ca (calcite, dolomite, or aragonite) at 8 kV and 2 kV (Fig. 4).

Utilization of low beam voltages also reduces radiation damage to the shale structure itself. For example, our experience demonstrates that morphologically distinct calcite fragments have been shown to be susceptible to degradation under a 5 kV beam while undergoing no apparent alteration at only 2 kV. An example of such degradation is shown in Figure 5. The images show an example of a calcite grain imaged at 2 kV with no apparent damage to the structure during several minutes of continuous scanning at 800 pA of beam current (Fig. 5a). Subsequent change to 5 kV and

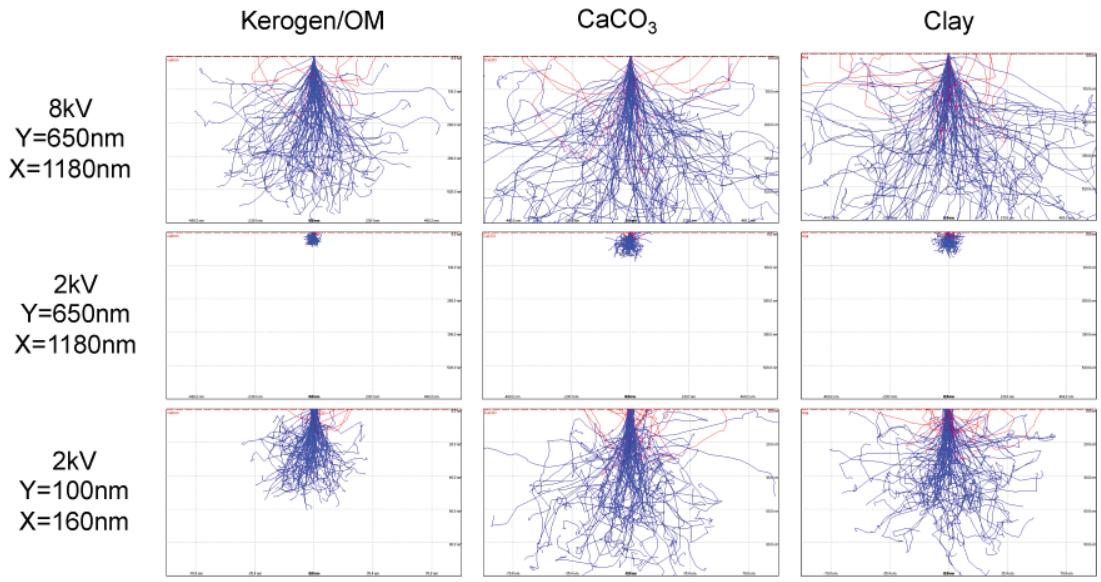

Figure 4. Monte Carlo simulations (CASINO) of secondary (blue) and backscattered (red) electron beam-specimen interactions in three components of shale—kerogen (OM = organic material), calcium carbonate, and clay—at both high (8 kV) and low (2 kV) beam accelerating voltages. The bottom row shows 2 kV simulation with an adjusted X, Y scale.

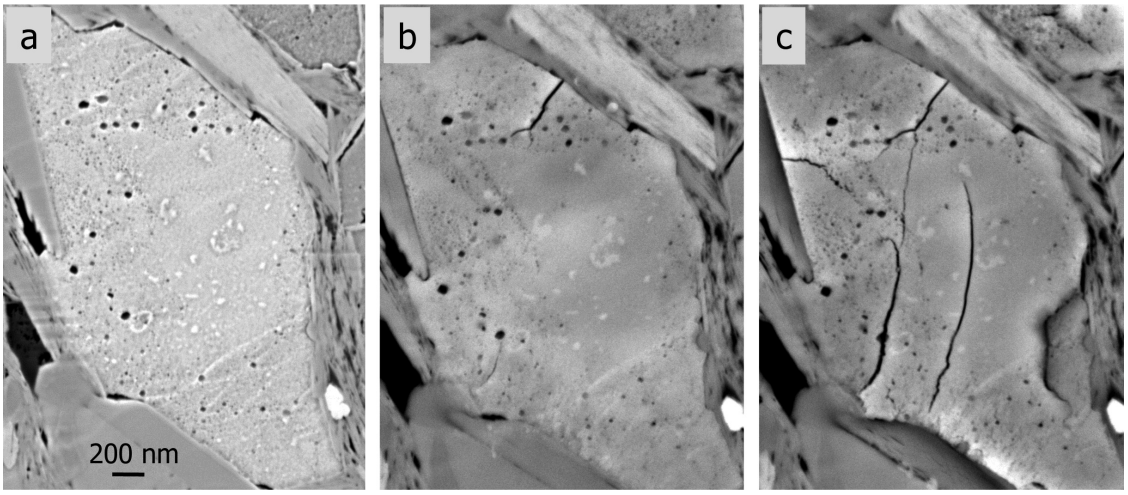

Figure 5. Calcite grain in shale imaged at (**a**) 2 kV versus the same grain imaged at (**b**,**c**) 5 kV. The 5 kV images show damage to the crystal developing over beam exposure time: (**b**) damage after first scan; (**c**) significant cracks and crystal shrinking developing after 10 scans. The sample was prepared using the JEOL Cross-Section Polisher.

800 pA starts to introduce cracks and voids into the grain, and the structure modification can be seen in subsequent scans (Figs. 5b, 5c). This observation reinforces the idea that lower voltage cannot only increase the spatial resolution of the CL detection but also preserve the original structure for the duration of the experiment.

Cathodoluminescence has been widely applied to geological research and can be used as a complimentary analysis along with EDS and WDS. For geological specimens the use of CL can often times help to easily differentiate between various constituents when the backscatter coefficient for those materials is fairly close (even down to the ppm level) where there is minimal difference in backscatter image contrast. Some components of the shale specimens (calcite, dolomite, quartz) have a distinct CL signature compared to the components that are optically inactive such as clays or kerogen; however, the same CL active components are typically very hard to distinguish by using strictly a BSE signal. For example, it has been previously demonstrated (Boggs & Krinsley, 2006) that the early, finely crystalline dolomites display low permeability, whereas the coarser late dolomites display high permeability and can be characterized with great detail by using CL. CL can also provide differentiation between secondary quartz that does not luminesce and primary (detrial) quartz that displays luminescence. Combined use of CL and EDS facilitates identification of these materials and can provide insight into the permeability characteristics of a particular shale deposit. Figure 6

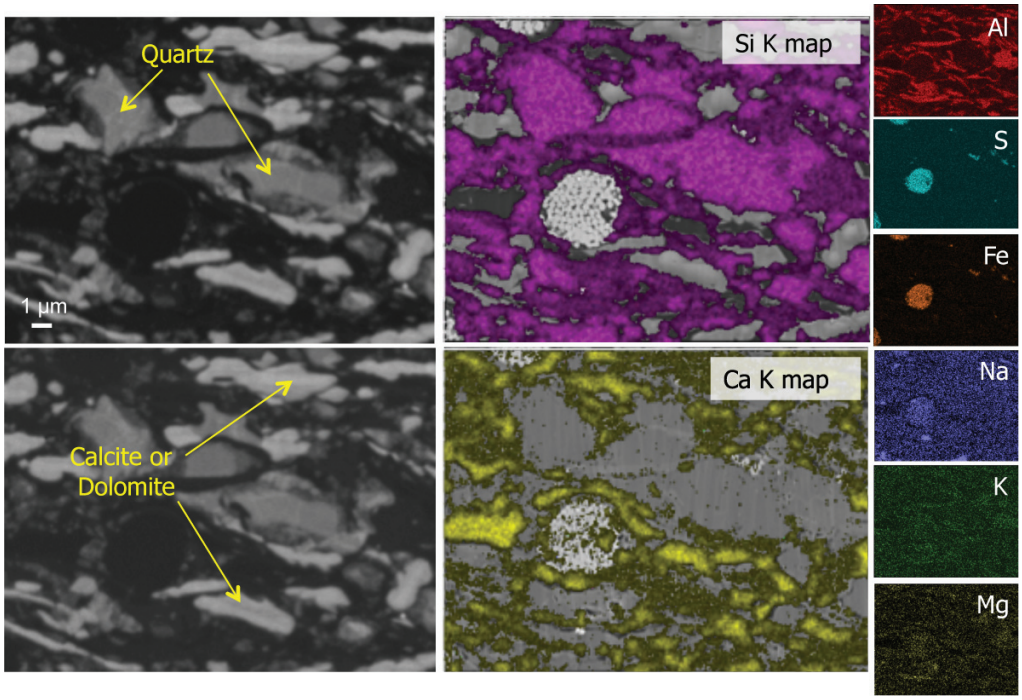

Figure 6. KE Centaurus CL images (left), overlaid BSE images–EDS maps (center), and remaining EDS surveys (right) of the Woodford sample, all acquired at 5 kV beam voltage.

shows an example of the Woodford shale analyzed with Oxford Instruments 50 mm^2 silicon drift detector EDS and imaged with the KE Developments CL detector. Even though the mineral differences are not obvious from the LABe image, it is fairly straightforward to correlate the location of carbonate (corresponding to Ca, C, and O elemental EDS maps) and quartz (Si and O maps).

Polycrystalline Diamond

Diamond is an allotrope of carbon and is well known for its remarkable chemical, physical, mechanical, and electrical properties (Field, 1992; Haggerty, 1999). Industrial grade diamonds are important due to their hardness and thermal conductivity properties, making them ideal as cutting and grinding tools. Polycrystalline synthetic diamond composite (referred to typically as PDC) has been widely used as a coating for tungsten carbide (WC) based drill bits for the oil and gas industry. The drill bit typically consists of synthetic diamond (with micron-sized grains) mixed with a metal phase (for instance, Co) and then sintered onto the cemented WC substrate. Understanding the structure of the diamond phase and its relationship to the properties, such as wear resistance, thermal stability, and conductivity, can determine the resulting usability and lifetime of a particular tool for a specific drilling application. Several groups have studied the PDC diamond materials in recent years (e.g., De et al., 2004; Boland & Li, 2010); however, they have relied on transmission electron microscope preparation for direct observation of the defect structures.

In our study we prepared PDC samples using the JEOL Cross-Section Polisher, which allowed previously unobtainable images of the diamond grains in SEM without any mechanical deformation that has in the past obscured any microstructural information other than grain size. Figure 7 shows a PDC specimen before and after CP preparation. Both images are taken with a secondary detector to show that the topography and relief present on the sample surface from the mechanical preparation is essentially eliminated using a 360° rotation holder accessory in the CP. This gives the researcher an opportunity to not only observe the general CL signal generated by the individual grains, but also to use a panchromatic detector to study the structural defects within the grains. Figure 8 shows a comparison of CL images from the PDC area at 2 and 5 kV, demonstrating yet again the advantage of using low kV for better spatial resolution. The images show that even at 5 kV accelerating voltage, the interaction volume is deep enough and wide enough to render the resulting CL image somewhat less sharp when compared to the 2 kV image of the same location. The linear features visible inside the grains correspond to planar microstructural defects, most likely due to the presence of twinning and/or slip planes (Brookes et al., 1999; De et al., 2004). Moreover, CL observation provides an additional feedback for improved backscatter imaging of crystal defects. Original examination of PDC samples with BSE detector at 5 kV and moderate probe current (~1 nA) under what would be considered normal brightness and contrast settings showed no obvious channeling or crystallographic contrast within the diamond grains (they essentially appear black as compared to the surrounding Co phase, which is white). However, based on observations from the CL images, a different set of parameters can be chosen for BSE imaging to enhance the crystallographic information. Figure 9 shows a comparison of a CL image

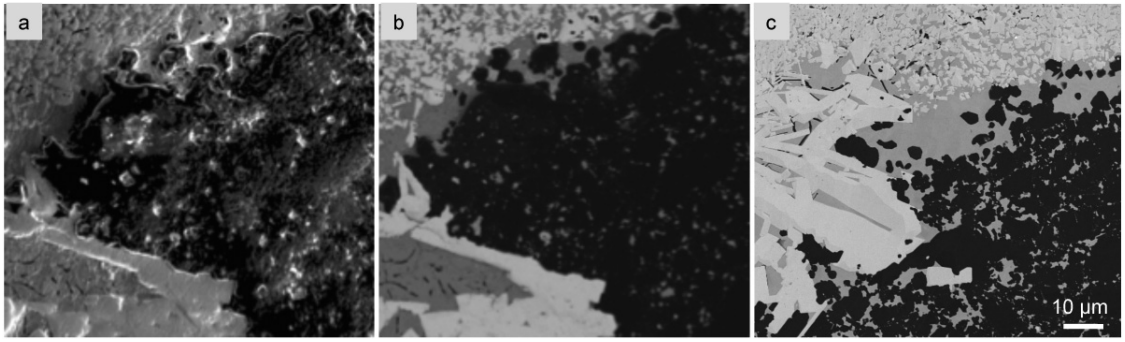

Figure 7. (**a**) Scanning electron (SE) and (**b**) BSE images of PDC mechanically polished prior to CP preparation. Black areas correspond to the diamond phase; lighter grains are WC substrate and Co phases. (**c**) SE image of CP polished sample, approximately the same area as in images **a** and **b**. Images taken at 5 kV.

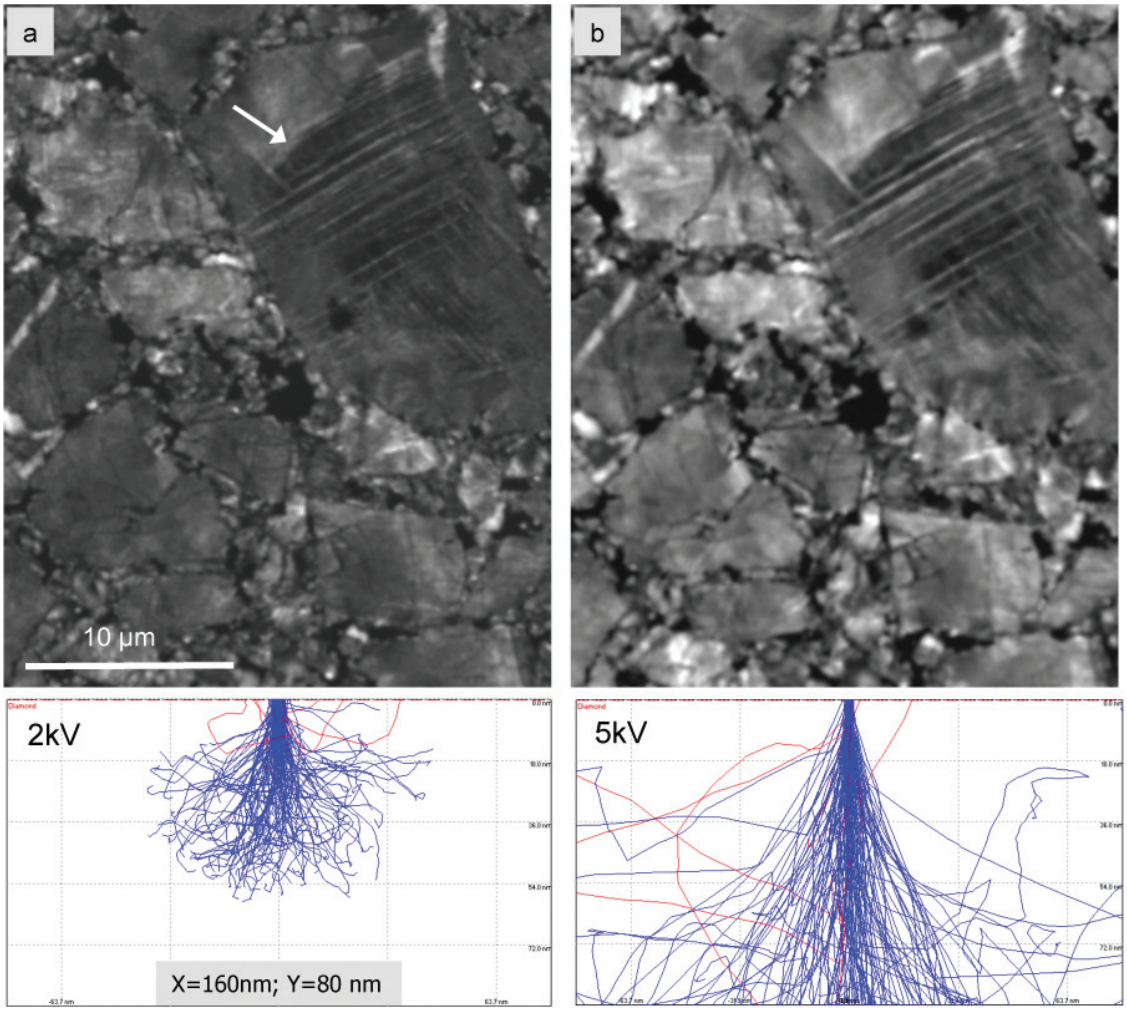

Figure 8. (**a**) 2 kV and (**b**) 5 kV CL images of PDC and corresponding Monte Carlo simulations of beam/specimen interaction (bottom). The arrow is pointing to characteristic planar defects observed throughout the specimen. Also note the overall increase in image sharpness at the lower kV. The scale is identical in both simulations.

and BSE image of the same grain, except this time a significantly higher probe (10 nA) current was utilized for imaging. This correlative approach between the different analysis and imaging techniques can provide the user with additional data points and information that would have been otherwise difficult to interpret.

Summary

For decades analysts have been fundamentally limited at or around the 1 μm size for any meaningful analyses. While lowering the accelerating voltage by even small amounts exponentially increased the spatial resolution of signals

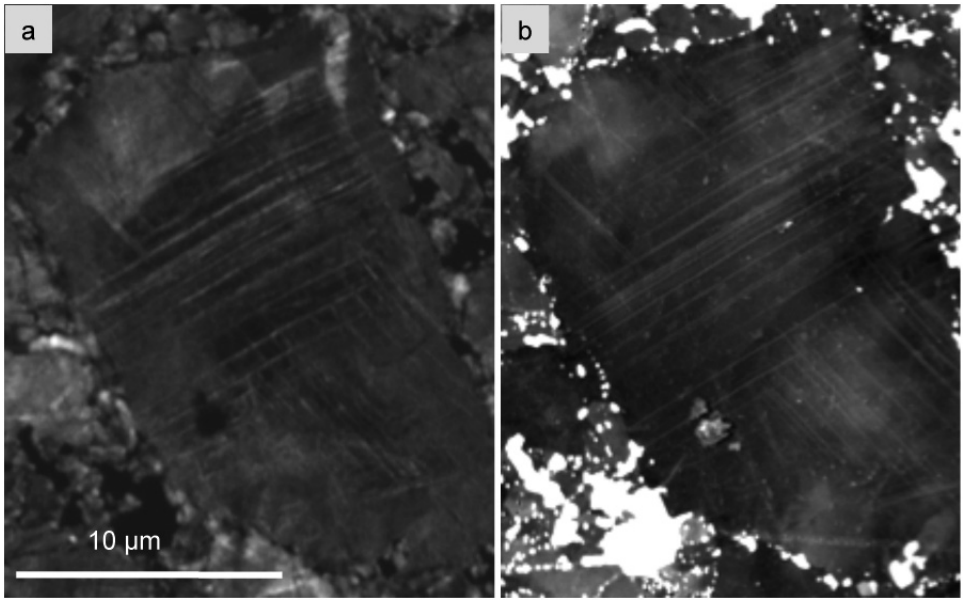

Figure 9. (**a**) 2 kV CL and (**b**) 5 kV high current (10 nA) BSE images of planar defects in diamond grains.

used in microanalysis, the combination of probe size limitation for sufficient signal and loss of probe size resolution at low accelerating voltages created this unavoidable limit. The introduction of Schottky field emission SEMs with their associated new lenses and automation that can create a small probe diameter, of the correct shape, with a large probe current, at low accelerating voltages has broken through this fundamental barrier allowing microanalysis (EDS, WDS, and CL) at the sub-100 nm level in bulk samples.

Acknowledgments

The authors would like to thank Nick Drenzek of Schlumberger-Doll Research Center for providing specimens for this analysis and fruitful discussions.

References

Boggs, S. & Krinsley, D. (2006). *Application of Cathodoluminescence Imaging to the Study of Sedimentary Rocks*. New York: Cambridge University Press.

Boland, J.N. & Li, X.S. (2010). Microstructural characterisation and wear behaviour of diamond composite materials. *Materials* **3**, 1390–1419.

Brookes, E.J., Greenwood, P. & Xing, G. (1999). The plastic deformation and strain-induced fracture of natural and synthetic diamond. *Diam Relat Mater* **8**, 1536–1539.

De, S., Heanley, P.J., Fei, Y. & Vicenzi, E. (2004). Microstructural study of synthetic sintered diamond and comparison with carbonado, a natural polycrystalline diamond. *Am Mineral* **89**, 438–445.

Erdman, N., Campbell, R. & Asahina, S. (2006). Precise SEM cross section polishing via argon beam milling. *Microsc Today* **14**(3), 22–25.

Field, J. (1992). *Properties of Natural and Synthetic Diamond*. London: Academic Press.

Haggerty, S. (1999). A diamond trilogy: Superplumes, supercontinents, and supernovae. *Science* **285**, 851–860.

Hovington, P., Drouin, D. & Gauvin, R. (1997). CASINO: A new era of Monte Carlo code in C language for the electron beam interaction—Part I: Description of the programme. *Scanning* **19**, 1–14.

Milner, M., McLin, R. & Petriello, J. (2010). Imaging texture and porosity in mudstone and shales: Comparison of secondary and ion-milled backscatter SEM methods. Publication 138975. Canadian Society for Unconventional Gas/Society of Petroleum Engineers.

Yacobi, B.G. & Holt, D.B. (1990). *Cathodoluminescence Microscopy of Inorganic Solids*. New York: Plenum Press.